Monte Carlo Methods and Applications, 115–123

Chapter 13

Monte Carlo Simulation of Asymmetric Flow Field Flow Fractionation

Oleg Iliev, Tigran Nagapetyan, and Klaus Ritter

Abstract. SDEs are used in the description of a variety of industrial processes. While numerous studies on Monte Carlo and multilevel Monte Carlo methods for SDEs used in financial engineering (option pricing, calculation of Greeks etc.) are available in the literature, technical applications are not so broadly studied. In this paper we briefly explain the Asymmetric Flow Field Flow Fractionation process for nanoparticle separation, introduce an SDE-based mathematical model, describe a Monte Carlo procedure for its solution, and end by presenting some numerical results.

Keywords. Multilevel Monte Carlo, SDE, Nanoparticle Transport and Separation, Asymmetric Flow Field Flow Fractionation.

2010 Mathematics Subject Classification. 65C05.

13.1 Motivation

The motion of small particles suspended in liquids is of great importance for a number of processes in medicine, biology, chemistry, etc. Our research, in particular, is motivated by the Field Flow Fractionation approach for segregation of small particles of two or more different sizes of submicron scale (for details see, e.g., [11] and references therein).

Monte Carlo methods and their modifications are suitable tools for the numerical simulation of such processes. The multilevel Monte Carlo method [6, 8], in the following denoted by MLMC, has already proven its efficiency for many financial problems where stochastic differential equations (SDEs) are used (see, e.g., [2,6,7]). Furthermore, suitable MLMC methods are almost optimal randomized algorithms for the quadrature of Lipschitz functionals of SDEs [5]. We extend the application of the MLMC method to the technical problem of nanoparticle separation, as we consider an SDE-based model for a dilute suspension of rigid noninteracting particles.

13.2 AFFFF

Asymmetric Flow Field Flow Fractionation, denoted hereon as AFFFF, is a special

CE Note 27: The quality of Figs. 13.1 and 13.2 is poor (low resolution bitmap). Can you supply better versions?

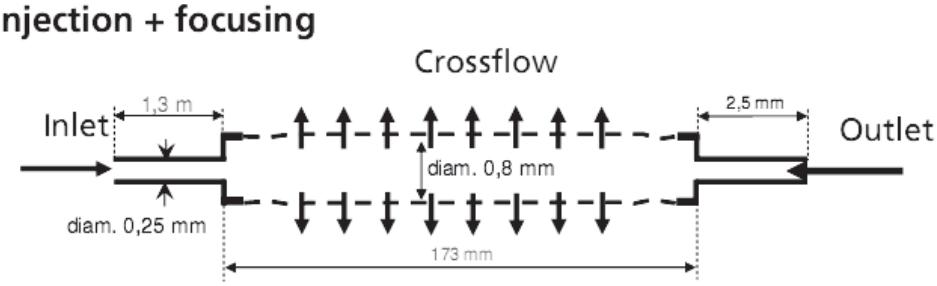

Figure 13.1. Hollow Fiber device during the focusing–injection stage for AFFFF.

case of the Field Flow Fractionation technique. During AFFFF the particles get separated according to their size, or more exactly, to their hydrodynamic radius. The fractionation relies on the interplay between laminar flow and Brownian diffusion. A horizontal flow of a solvent along a membrane is combined with a strong cross flow across the membrane. The membrane is impermeable for the particles, while the solvent can flow throughout it. Computer simulations of different AFFFF devices were performed by the authors, but due to the limited size of this chapter we will consider only a hollow fiber (HF) device.

AFFFF consists of two main stages: a focusing–injection stage and an elution stage.

Focusing–injection stage. An HF geometry and a sketch of flow directions during the focusing–injection stage can be seen in Figure 13.1. It should be noted that different scales for different parts of the device are used in the sketch. The axisymmetric HF, which is considered here, is 173 mm long itself (see the middle of the sketch), while the left capillary (serving to connect the HF to the sample reservoir) is 1300 mm long. During the focusing–injection stage, the solvent is entering the Hollow Fiber from both sides, and leaves through the membrane (see Figure 13.1). The ratio between the left and the right volumetric fluxes determines the position of the focusing line. The particles are injected from the left side during a certain time interval (shorter than the total duration of the focusing–injection stage), and they are transported towards the membrane due to the strong cross flow. On the other hand, the Brownian diffusion, which acts isotropically, prevents particles from resting at the membrane surface. The interplay between the force induced by the cross flow and the Brownian diffusion results in forming a boundary layer with average distance from the membrane depending on the particle size (i.e., on the diffusion coefficient) and on the intensity of the cross flow (see, e.g., [3,13]). Smaller particles with their larger diffusion coefficient form a layer which has a larger distance to the membrane.

At the end of the focusing–injection stage, the injected particles are located in a thin layer on the membrane, within a focusing zone around the focusing line, and this is the starting point of the consecutive horizontal transport of the particles.

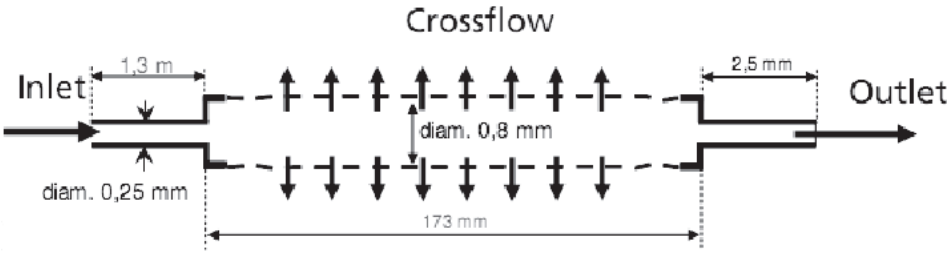

Figure 13.2. Hollow Fiber device during the elution stage for AFFFF.

Elution stage. A sketch of flow directions during the elution stage can be seen in Figure 13.2. Due to the parabolic profile of the horizontal velocity, a horizontal separation of the particles is achieved at a certain distance from the focusing line. During the elution stage, smaller particles are transported faster than the larger particles towards the channel outlet, because they experience a higher tangential flow velocity. For a more detailed description of AFFFF process see, e. g., [11,13].

13.3 Mathematical Model and Numerical Algorithm

13.3.1 Mathematical Model

The Navier–Stokes–Brinkman system governs the flow in the channel and in the porous membrane. The equations read as follows:

$$\begin{gathered} \frac{\partial \vec{V}}{\partial t} - \nabla \cdot \left(\nu \nabla \vec{V}\right) + \left(\vec{V}, \nabla\right)\vec{V} + \nu K^{-1} + \tfrac{1}{\rho}\nabla p = \vec{f} \\ \nabla \cdot \vec{V} = 0. \end{gathered} \tag{13.1}$$

Here $\vec{V} = (V_1, V_2)$, p, ν and ρ are the velocity, the pressure, the viscosity and the density of the fluid, respectively (see, e. g., [1,10]). Further on, K is the permeability of the membrane, which is considered as a porous medium here. In the pure fluid region K is set to infinity, which cancels the corresponding term, and (13.1) reduces to the Navier–Stokes system.

The particle transport in the pure fluid region $\mathcal{O} \subset \mathbb{R}^2$ is governed by the velocity field and by a stochastic term involving a 2-dimensional Brownian motion $\vec{W} = (W_1, W_2)$. The particle position $\vec{X} = (X_1, X_2)$ is a stochastic process with continuous paths taking values in $\overline{\mathcal{O}}$. This process is described by an SDE, driven by $\vec{W}$, with drift coefficient $\mu = \vec{V}$ and with a constant diffusion coefficient $\hat{\sigma} = diag(\sigma) \in \mathbb{R}^{2\times 2}$ for some diffusion parameter $\sigma > 0$. Since particles cannot penetrate the membrane, we consider all boundaries of the channel to be reflecting ones, except for the inflow

and the outflow boundaries. Here the reflection is understood in the sence of normal reflection (see [12]).

Equations of this type are called multidimensional Skorohod SDEs, and existence and uniqueness results for a strong solution are available under different assumptions on the domain $\mathcal{O}$ (and for more general driving processes). In particular, the assumptions from [12] are met in our application.

13.3.2 The MLMC Algorithm

We want to estimate the expectation $E(u(\vec{X}))$ of a square-integrable functional u on the path space of the Skorohod SDE via the MLMC method based on the Euler-Maruyama scheme.

At first the drift coefficient $\mu = \vec{V}$ has to be determined numerically. To this end the Navier–Stokes–Brinkman equations (13.1) are discretized by means of a finite volume method on an orthogonal nonuniform grid, which is exponentially refined close to the membrane. The solution procedure is rather standard and hence is not discussed here. For the simulation of the SDE by means of the Euler–Maruyama scheme, the respective values of the velocity field are obtained from the approximate values on the grid via local interpolation.

In the case of the SDE *without* reflection, the Euler–Maruyama scheme with an equidistant stepsize h has the form

$$\vec{X}^h_{k+1} = \vec{X}^h_k + h \cdot \mu(kh, \vec{X}^h_k) + \sigma \cdot (\Delta^h \vec{W})_k \quad k = 0, 1, \ldots, \tag{13.2}$$

where $(\Delta^h \vec{W})_k = \vec{W}((k+1)h) - \vec{W}(kh)$ is a Brownian increment. By piecewise linear interpolation and taking into account the reflection at the boundary the Euler–Maruyama approximation is extended to a process with continuous paths taking values in $\overline{\mathcal{O}}$, which will be denoted by $\vec{X}^h$.

Obviously,

$$\vec{X}^h = \varphi^h(\Delta^h \vec{W}),$$

where $\Delta^h \vec{W} = ((\Delta^h \vec{W})_0, (\Delta^h \vec{W})_1, \ldots)$ and where φ^h is defined by (13.2) accompanied by a proper reflection algorithm (see [4]). The functionals u to be considered in the sequel depend on an initial segment of $\vec{X}$, whose length is given by an almost surely finite stopping time. Likewise the computation of $u(\vec{X}^h)$ involves only finitely many Brownian increments for every h with probability one.

We choose integers $M > 1$ and $L \geq 1$, and we employ Euler–Maruyama approximations with different time steps $h_\ell = M^{-\ell}$ for $\ell = 0, \ldots, L$. With N_ℓ denoting the number of replications at level ℓ, and with independent copies

$$\vec{W}_{0,1}, \ldots, \vec{W}_{0,N_0}, \ldots, \vec{W}_{L,1}, \ldots, \vec{W}_{L,N_L}$$

of the Brownian motion $\vec{W}$, the MLMC estimator Y for $E(u(\vec{X}))$ is given by

$$Y = \frac{1}{N_0}\sum_{i=1}^{N_0} U_{0,i} + \sum_{\ell=1}^{L}\left[\frac{1}{N_\ell}\sum_{i=1}^{N_\ell}\left(U_{\ell,i} - U'_{\ell,i}\right)\right],$$

where

$$U_{\ell,i} = u\big(\varphi^{h_\ell}(\Delta^{h_\ell}\vec{W}_{\ell,i})\big)$$

for $\ell = 0, \ldots, L$ and

$$U'_{\ell,i} = u\big(\varphi^{h_{\ell-1}}(\Delta^{h_{\ell-1}}\vec{W}_{\ell,i})\big)$$

for $\ell = 1, \ldots, L$. Note that $U_{\ell,i}$ and $U'_{\ell,i}$ are coupled via $\vec{W}_{\ell,i}$, while $U_{\ell,i}$ and $U'_{\ell+1,j}$ are independent.

In general, Y is a biased estimator, since $E(Y) = E(u(\varphi^{h_L}(\Delta^{h_L}\vec{W})))$. With v_0 denoting the variance of $u(\varphi^{h_0}(\Delta^{h_0}\vec{W}))$, and with v_ℓ denoting the variance of $u(\varphi^{h_\ell}(\Delta^{h_\ell}\vec{W})) - u(\varphi^{h_{\ell-1}}(\Delta^{h_{\ell-1}}\vec{W}))$ for $\ell = 1, \ldots, L$, the variance of Y is given by $V(Y) = \sum_{\ell=0}^{L} v_\ell/N_\ell$. For the functionals u under consideration, the expected cost of Y is proportional to $\sum_{\ell=0}^{L} N_\ell/h_\ell$. According to [6], the minimization of $\sum_{\ell=0}^{L} N_\ell/h_\ell$ under the constraint $V(Y) \le \varepsilon^2/2$ for any given $\varepsilon > 0$ leads to

$$N_\ell = \left\lceil 2\varepsilon^{-2}\sqrt{V_\ell h_\ell}\left(\sum_{\ell=0}^{L}\sqrt{V_\ell/h_\ell}\right)\right\rceil. \tag{13.3}$$

The actual implementation of the MLMC algorithm involves bias estimates to appropriately choose the maximal level L and variance estimates to determine the number of replications per level; see (13.3). Furthermore, based on our numerical simulations experience we have chosen $M = 4$.

13.4 Numerical Results

In this section we will present some results from simulations of the focusing–injection and the elution stages of the AFFFF.

Simulation of the focusing–injection stage. The goal of the simulations, as defined by our industrial partner, is to study the dynamics of the injection of the particles, as well as the influence of the inflow control on the size and the shape of the focusing zone. Due to lack of space, only two snapshots of the injection process are shown here. Injection of smaller particles ($r = 3.2$ nm, Figure 13.3) and of larger particles ($r = 32$ nm, Figure 13.4) is simulated under the same flow conditions, and the snapshots are taken at the same time instance. Figures 13.3 and 13.4 only show half of the HF cross section, due to symmetry. The final shape of the focusing zone, which is not shown here, can be controlled by the inflow velocity.

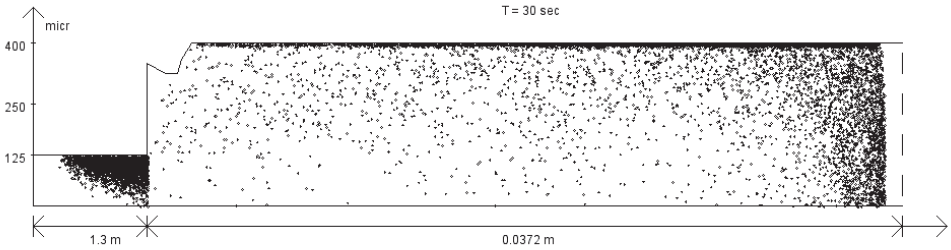

Figure 13.3. Particle injection, size $r = 3.2$ nm.

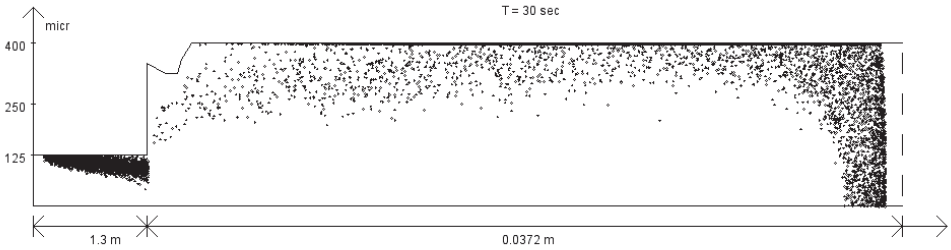

Figure 13.4. Particle injection, size $r = 32$ nm.

MLMC for restoring the diffusion coefficient at the focusing–elution stage. Let $\hat{X}_2$ denote the distance of a particle from the walls of the channel at the end of the focusing–injection stage. The cross flow $\hat{V}$ near the walls of the channel is almost a constant, so the distribution of the random variable $\hat{X}_2$ is well approximated by an exponential distribution with parameter $\hat{V}/D$, where $D = \sigma^2/2$ with σ denoting the diffusion parameter of the SDE. Recall that D depends on the particle size (see, e. g., [3]). The latter distribution is also known as a barometric distribution.

In order to check the consistency of our approach, we have employed the MLMC algorithm to obtain an empirical distribution of $\hat{X}_2$, which is then used to provide an estimate for D. The estimate is compared to the known value of D, which is calculated based on particles radius (see [3]). Results from numerical experiments with the MLMC algorithm are presented in Table 13.1.

Table 13.1. Multilevel Monte Carlo method for restoring the coefficient $D = 76.2\ \mu^2$/s. Cross flow equal to 30 μ^2/s.

Desired accuracy of MC simulation	*Absolute error*	*Relative error*
$\varepsilon = 10^{-3}$	$4.0 \cdot 10^{-1}$	$5.7 \cdot 10^{-3}$
$\varepsilon = 10^{-4}$	$9.8 \cdot 10^{-2}$	$1.4 \cdot 10^{-3}$
$\varepsilon = 10^{-5}$	$4.2 \cdot 10^{-2}$	$5.9 \cdot 10^{-4}$

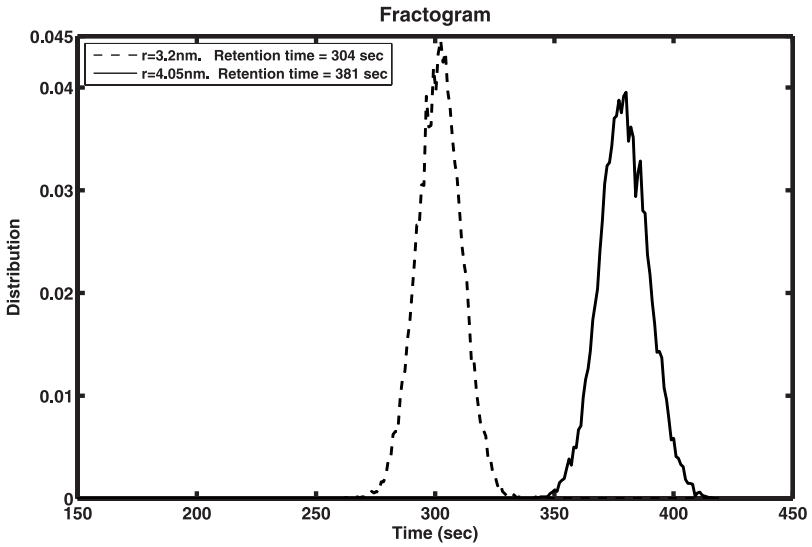

Figure 13.5. Fractogram for $r = 3.2$ nm and $r = 4.05$ nm, HF device.

Elution stage. The horizontal separation of the particles is actually done during the elution stage, and in practice the separation is evaluated from fractograms. Fractograms (see Figure 13.5) are a measure for the mass of particles that exit the outlet per unit time, and they serve as an approximation to the density of the distribution of the exit time of $\vec{X}$ from the channel. Ideally the fractograms of particles of different size should be 'well separated'. Additionally, the so-called retention times, which are the medians of the fractograms, should be 'small', as this indicates that the total duration of the separation process is small. We have employed a Monte Carlo algorithm to obtain fractograms via simulation. A particular goal of our simulations is to study the properties of the fractograms depending on different focusing and elution regimes. The results are summarized in Table 13.2. The retention time is computed for particles with $r = 3.2$ nm (fifth column) and $r = 4.05$ nm (last column) under different focusing regimes (first and third columns) and different elution regimes (fourth column). These results and the respective fractograms, which are not shown here, allow us to conclude whether or not the retention time can be reduced while keeping the fractograms well separated.

Exit times, in particular their distribution functions and quantiles thereof, play an important role in the present work. For SDEs without reflection the computation of expected exit times via classical Monte Carlo and MLMC algorithms is analyzed in [9].

Acknowledgments. The authors express sincere thanks to Dr. Johann and Dr. Schuch from Wyatt Technology Europe Ltd. for providing AFFFF data and for the useful

Table 13.2. Parameters of simulation (absolute values). Retention times (s) of particles with radius 3.2 and 4.05 nm.

Focusing time	*Parameter*	*Focusing [ml/min]*	*Elution [ml/min]*	$t_r = 3.2$ *nm*	$t_r = 4.05$ *nm*
	inlet	0.085	1.2		
V1 — 180 sec	outlet	0.765	0.35	308	387
	crossflow	0.85	0.85		
	inlet	0.17	1.2		
V2 — 180 sec	outlet	0.68	0.35	291	366
	crossflow	0.85	0.85		
	inlet	0.34	1.2		
V3 — 180 sec	outlet	0.51	0.35	255	322
	crossflow	0.85	0.85		
	inlet	0.17	0.775		
V4 — 180 sec	outlet	0.255	0.35	160	201
	crossflow	0.425	0.425		

discussions on the results, and to Mrs. Shklyar from Fraunhofer ITWM for her valuable help in performing the simulations. The research of O. Iliev and T. Nagapetyan is supported by BMBF project 03MS612D, "FROPT".

References

[1] P. Angot, Analysis of singular perturbations on the Brinkman problem for fictitious domain models of viscous flows, *Math. Methods Appl. Sci.* **22** (1999), 1395–1412.

[2] R. Avikainen, On irregular functionals of SDEs and the Euler scheme, *Finance and Stochastics*, **13** (1999), 381–401.

[3] R. Becker, *Theorie der Wärme*, Springer, Heidelberg, 1966.

[4] C. Costantini, B. Pacchiarotti, and F. Sartoretto, Numerical approximation for functionals of reflecting diffusion processes, *SIAM J. Appl. Math.* **58** (1998), 73–102.

[5] J. Creutzig, S. Dereich, T. Müller-Gronbach, and K. Ritter, Infinite-dimensional quadrature and approximation of distributions, *Found. Comput. Math.* **9**, 391–429, 2009.

[6] M. Giles, Multi-level Monte Carlo path simulation, *Operations Research* **56** (2008), 607–617.

[7] M. Giles, D. Higham, and X. Mao, Analysing multi-level Monte Carlo for Options with non-globally Lipschitz payoff, *Finance and Stochastics* **13** (2009), 403–413.

[8] S. Heinrich, Monte Carlo complexity of global solution of integral equations, *J. Complexity* **14** (1998), 151–175.

[9] D. Higham, X. Mao, M. Roj, Q. Song, and G. Yin, Mean exit times and the multi-level Monte Carlo method, Research Report, University of Strathclyde, 2011.

[10] M. Kaviany, *Principles of Heat Transfer in Porous Media*, Springer, New York, 1995.

[11] M.E. Schimpf, K.D. Caldwell, and J.C. Giddings, *The FFF Handbook*, Wiley, New York, 2000.

[12] Y. Saisho, Stochastic differential equations for multi-dimensional domain with reflecting boundary, *Probab. Th. Rel. Fields* **74** (1987), 455–477.

[13] K.-G. Wahlund and J.C. Giddings, Properties of an asymmetrical flow field-flow fractionation channel having one permeable wall, *Anal. Chem.* **59** (1987), 1332–1339.

Author information

Oleg Iliev, Fraunhofer Institute for Industrial Mathematics, Kaiserslautern, Germany; Technical University of Kaiserslautern, Germany; Institute of Mathematics, BAS, Sofia, Bulgaria.
Email: rami.haddad@fs.usj.edu.lb

Tigran Nagapetyan, Fraunhofer Institute for Industrial Mathematics, Kaiserslautern, Germany; Technical University of Kaiserslautern, Germany.
Email: Rana.Fakhereddine@etu.univ-savoie.fr

Klaus Ritter, Technical University of Kaiserslautern, Germany.
Email: Christian.Lecot@univ-savoie.fr